JJBS

Volume 17, Number 3,September 2024
ISSN 1995-6673
Pages 471 – 480
https://doi.org/10.54319/jjbs/170309

Jordan Journal of Biological Sciences

# The Evaluation of the Antifungal activity of Chitosan Nanomolecules laden with *Trichoderma harzianum* Extract on *Fusarium oxysporum* f.sp. *lycopersici*

Rasha Khalid Hussein AL-Masoudi*, Neamat J. AL Judy

*Department of Biology, College of Science, Baghdad University, Baghdad, Iraq.*

*Received: December 26, 2023; Revised: February 16, 2024; Accepted: February 22, 2024*

**Abstract**

The economic repercussions of Fusarium wilt on global tomato crops underscore the disease's paramount importance. And by employing non-toxic, environmentally friendly ingredients that align with sustainable practices and emphasize biosafety considerations, green synthesis, an emerging field in nanobiotechnology, presents financial and ecological benefits surpassing customary chemical and physical approaches. The main objective of the present investigation is to formulate chitosan nanomolecules laden with *Trichoderma harzianum* extract and characterize them. Additionally, the study aimed to investigate the antifungal effectiveness of these chitosan nanomolecules towards *Fusarium oxysporum* f.sp. *lycopersici*. Employing the ionic gelation technique and tripolyphosphate (TPP), chitosan nanomolecules laden with *T. harzianum* extract were synthesized. Subsequent characterization involved UV-vis, FTIR, AFM, SEM, XRD, and EDX techniques to demonstrate the effectiveness of the biochemical transformation. In addition, the antifungal efficacy of bio-manufactured chitosan nanomolecules has been assessed against five strongly virulent isolates from *F. oxysporum* f.sp. *lycopersici*. The study revealed the highest inhibition rates of growth for all isolates to be 100% at a 1 mg/ml concentration of CNPs. In contrast, the minimal inhibitory level rates at 0.125 mg/ml of CNPs were 32.75, 32.83, 32.85, 36.92, and 41.17%, consecutively. This investigation's findings have revealed a recently discovered biological pathway to biosynthesize chitosan nanomolecules in an environmentally friendly way by using *T. harzianum*. The confirmed antifungal efficacy of the synthesized CNPs towards *F. oxysporum* suggests their potential as alternatives to or reducers of widespread fungicide use, applicable across various technical and agricultural domains.

**Keywords**: Chitosan nanomolecules, Fusarium wilt, Ionic gelation, Tomato plant

## 1. Introduction

One of the globally significant and extensively consumed vegetables, particularly in Iraq, is the tomato (*Lycopersicon esculentum* Mill) (Al-dobaissi, and Al-masoudi, 2021). The soil fungus Fusarium is a facultative parasitizer that favors parasitizing live tissues over saprophytic ones. Although it can be found in various kinds of soils, sandy soils are thought to be the best for its development. When there is no host present, it can live in the soil for ten to fifteen years (Hashim *et al.,* 2023). *F. oxysporum* f. sp. *lycopersici* pathogenicity first targets the roots. After that, the vascular fabric colonizes and results in severe necrosis, aerial chlorosis, and wilting. Certain species yield poisons, such as fusaric acid, which first infects the floral tissue during anthesis and then spreads across the inflorescence's central axis, harming and contaminating grains (Fradi, 2022).

The successful cultivation of tomatoes faces various challenges, among which Fusarium wilt stands out as a noteworthy concern, attributed to *Fusarium oxysporum* f. sp. *lycopersici*. In the context of diseases and crop productivity losses, fungi exert a more pronounced influence compared to other plant parasites (Juber, 2012). Chemical fungicides can eliminate plant pathogenic fungi; however, their excessive use gives rise to multiple adverse effects (Abdullah *etal*., 2019). These include the degradation of soil quality, disturbance of the natural balance of flora and fauna, escalation of infection resistance, and contamination of the surrounding environment (Fradi, 2022). As one of the world's most sustainable control methods, biological control is strongly advised and supported (Jasim *et al*., 2022).

*Fusarium* crown and root rot disease may be suppressed by biological control agents (Abed *et al*., 2021). A common presence in soil, root, and foliar ecosystems, *Trichoderma harzianum* Rifai is a potentially useful tool for biological control; it can effectively combat numerous soil-borne pathogenic fungi, including strains of *Fusarium* (Kareem and Al-Araji, 2021). By competing with pathogens for resources, colonizing root surfaces, mycoparasitism, and other strategies, *T. harzianum* can directly provide biocontrol. Consequently, to improve crops and biocontrol soil-borne fungal infections, *T. harzianum* has become one of the most extensively used beneficial fungi (Esmael *et al*.,2021).

Nanotechnology has become a vital technology across many disciplines due to recent advancements in the production of diverse nano molecules that vary in

* Corresponding author. e-mail: rasha.khalid@sc.uobaghdad.edu.iq.

dimension, form, and action. In contrast to bulky substances, nanoparticles possess a higher specified external space as well as a greater reaction efficacy and, therefore have been demonstrated to affect a variety of live cells, including fungal cells. Green synthesis of nanomolecules has various advantages over physical and chemical techniques (Zhao *etal*., 2023). For the synthesis of nanoparticles in a variety of applications, chitosan has frequently been a preferred solution; it is a naturally occurring polysaccharide biopolymer, and the most well-known form is an amino polysaccharide derived cellular walls for insects, crustaceans, and fungal (Mustafa and Al –Ogaidi, 2023).

The use of Nano natural polymers is becoming more and more popular as a means of phytopathogenic fungi; this could provide a safe alternative to chemical fungicides and reduce the toxicity of metal nanoparticles (MNPs) (Medda *et al*., 2015). Out of all known nano-polymers, chitosan nanoparticles (CNPs) are drawing considerable attention for their application as the antifungals of choice for various pathogenic fungi. This interest is attributed to their unique characteristics, including non-toxicity, efficiency, biodegradability, high permeability, and broad-spectrum mycotoxic towards diverse phytopathogenic fungi (Oh *etal*., 2019). The primary objective of the current study has been to synthesize and characterize chitosan nanoparticles laden by using *T. harzianum* extract. Furthermore, the study aimed to assess the mycotoxic efficiency of these nanoparticles towards *F. oxysporum* f.sp. *lycopersici.*

## 2. Materials and methods

### *2.1. Fungal pathogen isolation, identification*

The present investigation focused on *F. oxysporum* f.sp. *lycopersici* which leads to Fusarium wilt disease. This fungus has been isolated from infected tomato plants between August and December 2022, and in January 2023 sourced from fields and greenhouses in Al-Rashidiya, Al-Zaafaraniya, Al-Mahmoudiya, Al-Nahrawan, Al-Taji, Al-Swayrah, and Karbala, Iraq. The symptoms that appeared on the shoots and roots of the infected plants in a field included yellowing and drooping leaves, the death of some branches, reddish-brown streaks that appeared in the vascular tissues of the stem when sliced with a knife, and finally, the death of the plants. Collected samples were individually sealed in plastic bags with the name of the location and the date of collection recorded on each bag. The pathogens were isolated and then identified from infected samples in the lab. Five parts of each infected plant (two for the root and three for the stem) were subjected to surface sterilization with a 1% hypochlorite solution, and subsequently cultured in Petri dishes with sterilized Potato Dextrose Agar (PDA), with a 5-day incubation period at 25 ± 2 °C. After obtaining pure cultures on the PDA medium using a single-spore method, they were stored at 4 °C until required (Farahani *etal.*, 2020). According to the morphology of the colony, conidiophores, and spore forms were used to identify *Fusarium* isolates in the lab. All fungal isolates were cultivated and preserved on autoclaved PDA and incubated for five days at 25±2 °C (Awad *et al*., 2020). Moreover, slant cultures were created, and all were kept in a refrigerator at 4 °C (Hussain e*t al*., 2022). The molecular and morphological characterization of isolates had been addressed in another accepted research done by the same researchers. The selection of five pathogenic isolates of *F. oxysporum* has been based on pathogenicity tests, prioritizing those exhibiting the highest severity.

### *2.2. Preparation of T.harzianum Crude Extract*

*T.harzianum* isolate was obtained from the Department of Agricultural Research in Baghdad and was diagnosed morphologically, and its diagnosis was also confirmed by molecular methods. For the preparation of *T. harzianum* extract, a 10 mm diameter mycelial agar disc has been taken from the mature layer of a 120-hour-old *T. harzianum* culture on Potato Dextrose Agar (PDA). This disc has been subsequently transferred to a 500 ml flask containing 300 ml of autoclaved Potato Dextrose Broth (PDB). The flask was then subjected to a ten-day incubation period at 27±2˚C on a shaker incubator operating at 150 rpm. Following incubation, the fungal cultures underwent centrifugation at standard measures, and the resulting extract was concentrated using a rotary evaporator (Mahdavi *etal*., 2013).

### *2.3. Preparation of Chitosan/T. harzianum Nanoparticles*

Using the same procedures mentioned in the references (El Naggar *etal*., 2022), the formulation of the chitosan-*T. harzianum* adduct involved the following procedures: Chitosan and 5% of *T. harzianum* extract were combined in equimolar ratios, and the calculated amount of water was removed. An intensification reaction has been conducted using a Dean-Stark (Clevenger) device using xylene. The chitosan amide product underwent repeated washing with methanol, ethanol, and warm distilled water. Afterward, the material was dried using a 50°C temperature, resulting in the production of a chitosan amide derivative.

The Chitosan NPs laden with *T. harzianum* extract were obtained using the ionic gelation pathway following the procedure outlined below (A 1% w/v), acetic acid solution has been employed to dissolve 5 mg/ml of the Chitosan-*T. harzianum* extract until the solution achieved transparency. Subsequently, a solution of Tri polyphosphate has been incrementally added to the Chitosan-*T. harzianum* extract solution in a 1:2.5 (w/w%) ratio, with constant mixing at room temperature for six hours. The resulting nanoparticles underwent separation; multiple wishing, removal of the supernatant layer, re-suspension of the precipitate in water, and subsequent drying (Agarwal etal., 2018).

### *2.4. Characterization of CNPs laden T. harzianum extract*

CNPs loaden *T. harzianum* extract has been characterized using UV-visible spectrum, FTIR, XRD, AFM, EDX, and SEM.

#### *2.4.1. UV-Visible Absorption Spectroscopy*

The absorbance spectrum of the chitosan nanoparticles (CNPs) incorporating *T. harzianum* extract has been determined utilizing UV-VIS double-beam spectrophotometers, covering a 200 to 800 nm range, to measure the absorption (Oh *et al*.,2019).

*2.4.2. Fourier Transform Infrared (FTIR) Test:*

Analyzing the functional groups present on the chitosan nanoparticles (CNPs) laden with *T. harzianum* extract and the extract itself has been accomplished through Shimadzu Fourier Transform Infrared Spectroscopy (FTIR). Spectra have been scanned with a resolution of 4 $cm^{-1}$ within the range of 400–4000 $cm^{-1}$. Standard sample preparation methods were employed, involving the dispersion of samples on a microscope slide (Dheeb *et al*., 2015).

*2.4.3. Atomic Force Microscopy (AFM)*

The shape of the nanoparticles' top layer has been seen using Atomic Force Microscopy (AFM) in Contact mode under ambient atmospheric conditions. The analysis has been conducted following established methodologies and procedures (Thomas *etal.,* 2017).

*2.4.4. X-ray diffraction (XRD)*

A thin layer of nanoparticles dispersed in a homogeneous water medium has been deposited onto a glass slide and allowed to undergo drying. Subsequently, an X-ray diffractometer, configured in 2θ/θ scanning mode with operational parameters set at 40 kV voltage, 30 mA current, and Cu K (α) radiation (λ = 1.540), has been employed to generate an XRD pattern (23). Data acquisition occurred with a step size of 0.0200 degrees over the 2θ range from 10 to 80 degrees. The analysis of Chitosan nanoparticles (CNPs) involved the interpretation of the XRD results using the JCPDS reference. The application of the Scherer equation facilitated the determination of particle sizes in the produced samples (Dheeb *etal.*, 2023).

*2.4.5. Analysis of Scanning Electron Microscopy (SEM*

Analyzing the top layer of the synthesized nanoparticles has been conducted using Scanning Electron Microscopy (SEM). A Brucker SEM instrument has been employed for the characterization of the morphology of CNPs laden with *T. harzianum* extract. Sample preparation adhered to established procedures (Abed *et al.*, 2021).

*2.4.6. Energy Dispersive X-ray (EDX)*

EDX test has been conducted utilizing EDX devices, which are employed in conjunction with a Scanning Electron Microscope (SEM) operating in transmission mode (Khan *et al.***,** 2019).

*2.5. Antifungal Activity of Chitosan NPs Laden T. harzianum Extract.*

The test has been designed to explore the in vitro antifungal efficiency of CNPs-laden *T. harzianum* extract towards *F. oxysporum* f.sp. *lycopersici*. The test has been performed in Petri dishes comprising sterilized Potato Dextrose Agar (PDA). Specific quantities of CNPs-laden *T. harzianum* extract were dissolved in deionized distilled water under aseptic conditions with stirring for 90 minutes. After adding the nanomaterial to PDA, the ultimate concentrations were achieved (0.125, 0.25, 0.5, and 1 mg/ml). To concoct the inoculum of the fungus, *F.oxysporum* mycelium has been transferred onto PDA plates extracted from a single colony (Huang *et al.*, 2021). A fungal disc with a diameter of 5 mm has been obtained from the pure and active growth periphery placed in the middle of the plates. Daily check-ups were conducted on the inoculated plates till the CNP-free control treatment reaches the margins of the plates. The antifungal efficacy has been compared with that of the commercial Topsin fungicide (with the active ingredient Thiophanate Methyl at 70%) regarding the mycelial outgrowth of *F. oxysporum* under identical conditions. Three replicates were conducted for each concentration with an additional three replicates for both the positive and negative control treatments. The inhibition of fungal growth has been evaluated using the formula below:

"Percentage inhibition of radial growth (PIRG) (٪) = [(A1-A2)/A1] × 100٪ "

A1 denotes the *F. oxysporum* radial growth in the control plate, and A2 denotes the *F. oxysporum* radial growth in the treatment plate (EL Sayed *et al*., 2023).

*2.6. Statistical Analysis:*

For the evaluation of the effect of different elements on this investigation's variables, the SAS software has been used (SAS, 2018). In the present investigation, the ANOVA test known as the least significant difference (LSD) has been employed to compare the means.

## 3. Results and Discussion

*3.1. Morphological Identification of Fusarium isolates*

Pathogenic *Fusarium* isolates were purified and identified using morphological and microscopic characteristics. The morphological characteristics of *Fusarium* isolates were observed on PDA media, such as cottony mycelium growth and changing color according to age, from a colony with pinkish violet colors to white, and cream-colored colonies. Characteristics of *F. oxysporum* observed under a microscope revealed that macroconidia have sickle-shaped, three to five septate, and basal cells with a foot shape. Microconidia are oval to reniform, without septa, in addition to the chlamydospores, as seen in culture. These features matched with *F. oxysporum* and were in concord to (Fradi, 2022).

*3.2. The Synthesized CNPs' Primary disclosure*

The present investigation focuses on a new fabrication of Chitosan NPs from chitosan solution utilizing *T. harzianum* extracts. No previous study on the application of the fungus *T. harzianum* for the transformation of chitosan polymers into nanoforms. As a result, the present investigation employs *T. harzianum* extract to establish a new methodology for the eco-friendly manufacturing method of CNPs. This process offers several advantages compared to the standard biosynthesis techniques (Abdulbaqi *et al.,* 2018).

*3.3. Characterization of CNPs Laden with T.harzianum Extract*

*3.3.1. UV-Vis Spectroscopy*

The UV-Vis spectrum depicted in Figure 1 for the *T. harzianum* extract reveals a singular peak at 254 nm, exhibiting an absorbance of 0.843. This peak is attributed to the π–π* and n–π* transitions within the characteristic category of organic compounds in the fungal extract. The presence of this broad peak is solid evidence affirming the efficacy of the fungal extraction method (Salih *et al*.,

2022).According to Figure 2, the spectrum of UV-Vis for CNPs laden with *T. harzianum* extract showed a characteristic peak at 297 nm with an absorbance of 0.72. The observed shift in UV-Vis spectrum stands as substantial evidence of the chemical reaction; consequently, this technique provides robust confirmation of the formation of a new material (Dheeb *etal*., 2019).

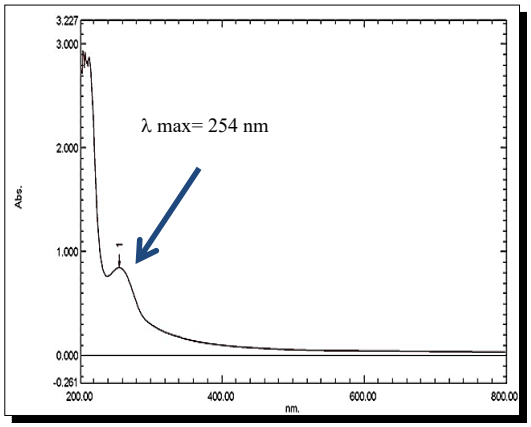


**Figure1.** UV-visible spectroscopy of *T.harazanium* extract with a peak at 254 nm ,and analyzed through a UV/VIS'S spectra range of 200–800 nm

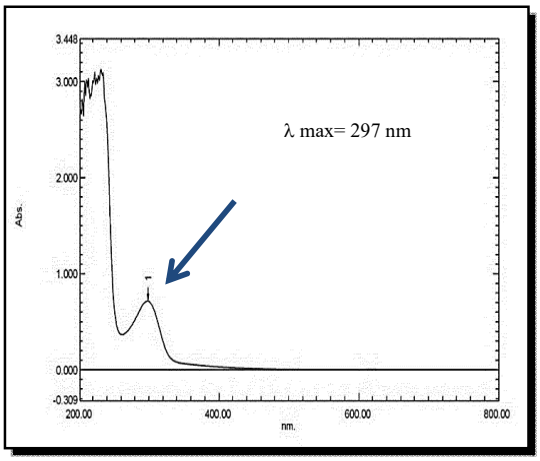


**Figure2.** UV- visible spectroscopy of CNPs laden with *T.harazanium* extract with a peak at 297 nm, ,and analyzed through a UV/VIS'S spectra range of 200–800 nm

### *3.3.2. Fourier Transform Infrared (FTIR) Analysis:*

The FTIR spectrum presented in Figure 3 for the *T. harzianum* extract reveals characteristic peaks corresponding to the functional groups of the organic compounds within the extract. The peak observed at 3390.86 $cm^{-1}$ is attributed to the OH group's stretching vibration in cis-aconitic anhydride, butyn-1-ol, 2-pyrrolidine thione, and decanoic acid, as indicated by the GC-MS results. The peak at 2939.52 $cm^{-1}$ corresponds to the stretching vibration of aliphatic C-H in the compounds. The presence of carboxylic acid is indicated by the peak at 2322.29 $cm^{-1}$, associated with the stretching vibration of C=O. The peak at 1608.63 $cm^{-1}$ is attributed to the C=C cyclic alkene. Additionally, the peak at 1402.25 $cm^{-1}$ is associated with the stretching vibration of S=O, indicative of Sulfonyl chloride. Peaks observed at 1327.03 and 1247.94 $cm^{-1}$ are attributed to the stretching of C-N, signifying aromatic amines. The C-O stretching of primary alcohol may be responsible for the peak at 1064.71 $cm^{-1}$. Peaks at 927.76, 860.24, 817.82, and 775.38 $cm^{-1}$ are assigned to the N-H wagging of amine compounds' stretching vibration. Lastly, the C-Br group's stretching vibration in alkyl halide compounds is identified as the origin of the peaks at 617.22 and 551.64 $cm^{-1}$.

The FTIR spectrum depicted in Figure 4 for Chitosan nanoparticles (CNPs) laden with *T. harzianum* extract exhibits characteristic peaks. The initial peak, identified at 3437.15 $cm^{-1}$, corresponds to the vibratory stretching of the OH bond of alcohol. Subsequently, the second peaks observed at 2924.09 and 2854.65 $cm^{-1}$ are attributed to the stretching vibrations of aliphatic C–H group'. Peaks at 1788.01 and 1714.72 $cm^{-1}$ are associated with the presence of the C=O stretching in conjugated acid halide and unsaturated ester. The absorption peak at 1651.07 $cm^{-1}$ is linked to the C=C stretching of the alkene group. The peak at 1381.03 $cm^{-1}$ is attributed to the wagging of CH3. The presence of the (C-O-C) bridge's anti-symmetric stretching is denoted by the peak at 1143.79 $cm^{-1}$, while the stretching vibration associated with the C–O group is indicated by the peak at 958.62 $cm^{-1}$. The stretching vibrations of the C-Cl group in alkyl halide compounds contribute to the peaks observed at 837.11, 623.01, and 511.14 $cm^{-1}$.

Demchenko *et al.* (2020) reported that the variable position chemical groups showed successful loading meaning the successful loading process of *T. harazanium* into chitosan/TPP and the formation of CSNPs loaded with *T. harazanium*. These results were confirmed by Alqaysi *etal* (2016), who demonstrated that shifted peaks indicate the formation of a new compound and thus changes in the functional groups of bioactive molecules suggested that they were related to the formation of *T. harazanium*-loaded CSNPs.

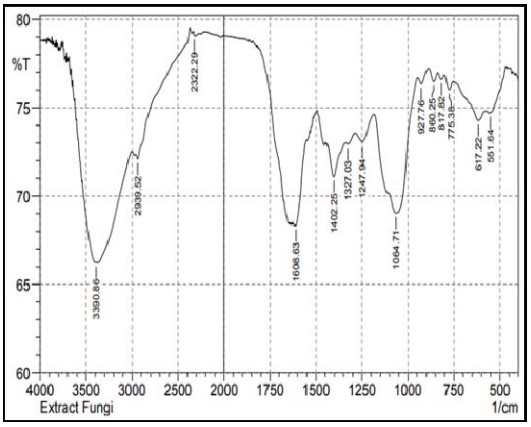


**Figure 3:** FTIR spectrum showed functional group of *T.harazanium* extract, spectra have been scanned with a resolution of 4 $cm^{-1}$ within the range of 400–4000 $cm^{-1}$.

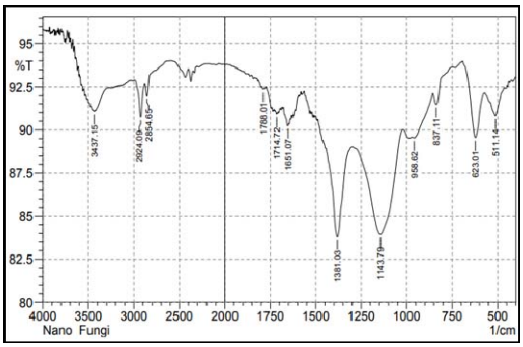


**Figure 4**: FTIR spectrum showed functional group of CNPs loaded with *T.harazanium* extract, spectra have been scanned with a resolution of 4 $cm^{-1}$ within the range of 400–4000 $cm^{-1}$.

### *3.3.3. X-ray diffraction (XRD)*

The XRD pattern is thought to be the distinctive mark of periodical atomic structures in any particular material. XRD analysis is a quick procedure that is mostly utilized in the discipline of material science, in the stage of determining the crystalline structure; moreover; it can provide data about the measurement of unit cells. The XRD of CNPs laden with *T. harzianum* extract in Figure 5 showed the characteristic peaks of nanochitosan at 11.625, 19.225, 22.975, 25.225, 33.525, and 38.975 degrees.

Furthermore, the measurement showed other peaks that could be attributed to the compounds of *T. harzianum* extract at 14.825, 29.375, 29.775, 35.375, 42.475, 46.925, 47.875, and 31.875 degrees. Depending on the Scherrer equation, the particle size has been calculated and found in the range 8.12-42.80 nm with a typical particle size of 22.68 nm, as illustrated in Table 1. These findings were consistent with those of Thamilarasan *et al*. (2018), who discovered that the pure chitosan diffraction peak, which had previously been discovered at 20.20°, had moved to a lower value of 19.85°. This migration may have been caused by the interaction between CS-NPs and TPP as well as the crystalline structure of CS-NPs. The patterns' variations may be related to changes in the crystal lattice's molecular arrangement (Morsy, 2019). The presence of both Nano chitosan and fungi extract peaks is solid evidence for the success of the reaction between the two starting materials.

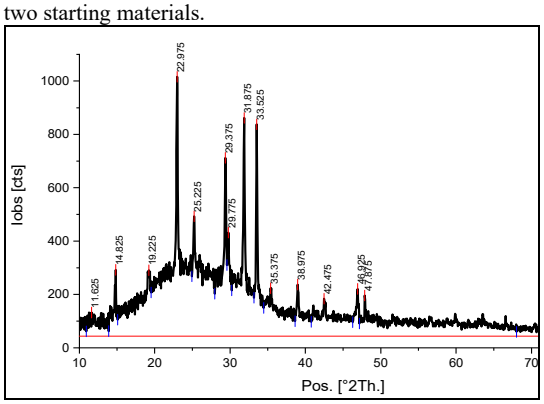


**Figure 5**. XRD of CNPs loaded with *T.harazanium* extract showed the five characteristic peaks of nanochitosan and eight characteristic peaks of fungal extract, X-ray diffractometer, configured in 2θ/θ scanning mode with operational parameters set at 40 kV voltage, 30 mA current, and Cu K (α) radiation (λ = 1.540)

**Table 1**. XRD data, particle size, and average particle size of CNPs laden with *T.harzianum*

| Peak position (degree) | Assignment | Height (Counts) | FWHM (degree) | Particle size (nm) | Average particle size (nm) |
|---|---|---|---|---|---|
| 11.625 | *CS | 88.8945 | 0.56161 | 14.86 | 22.68 |
| 14.825 | *FE | 248.7567 | 0.2338 | 35.82 | |
| 19.225 | CS | 247.5352 | 1.03677 | 8.12 | |
| 22.975 | CS | 972.4502 | 0.26067 | 32.51 | |
| 25.225 | CS | 449.5584 | 0.79469 | 10.71 | |
| 29.375 | FE | 668.5985 | 0.28233 | 30.40 | |
| 29.775 | FE | 388.5954 | 0.6 | 14.32 | |
| 31.875 | FE | 818.4524 | 0.2631 | 32.82 | |
| 33.525 | CS | 794.59 | 0.20264 | 42.80 | |
| 35.375 | FE | 179.8877 | 1.82232 | 4.78 | |
| 38.975 | CS | 193.8549 | 0.39316 | 22.40 | |
| 42.475 | FE | 140.4034 | 0.65992 | 13.50 | |
| 46.925 | FE | 177.4748 | 0.44537 | 20.33 | |
| 47.875 | FE | 152.693 | 0.26553 | 34.22 | |

* CS refer to Nano chitosan *FE refer to Fungal extract

### *3.3.4. Energy Dispersive X-ray (EDX)*

The EDX accounted for CNP load with *T. harzianum* extract (Figure 6) and showed five main peaks at 0.277, 0.432, 0.525, 1.041, and 3.312 KeV which attributed to the carbon, nitrogen, oxygen, sodium, and potassium, consecutively. The presence of these elements could be considered additional evidence for the formation of CNPs laden with *T. harzianum*. Furthermore, the EDX measurement showed one additional peak of Au (used in the sample preparation) at 2.250 keV.

The constituent parts of CNPs were examined using an electron microscope in conjunction with an EDXS study. When an electron beam from a scanning electron microscope (SEM) strikes an element's inner orbit, another electron from an outer orbit moves into the vacancy to fill it. This process results in the liberation of an energy variation that is specific to that element and manifests as an X-ray. Furthermore, there is a direct correlation between the particle's amount of the element and the intensity of the particular X-ray. Nonetheless, the analysis gives a positive result of the native chitosan's different elemental compositions, assuring the consistency and sustainment of CNPs throughout the biological conversion procedure (Thamilarasan *et al*. 2018). The outcomes concur with those of Raza and Anwar (2017), who verified the existence of CSNPs on the treated fabric using scanning electron microscopy outfitted with EDX. Furthermore, the Energy Dispersive X-ray Spectroscopy (EDX) spectrum of CS10 has four types of elements: C, O, N, and Br, according to Dheeb *et al*.( 2022).

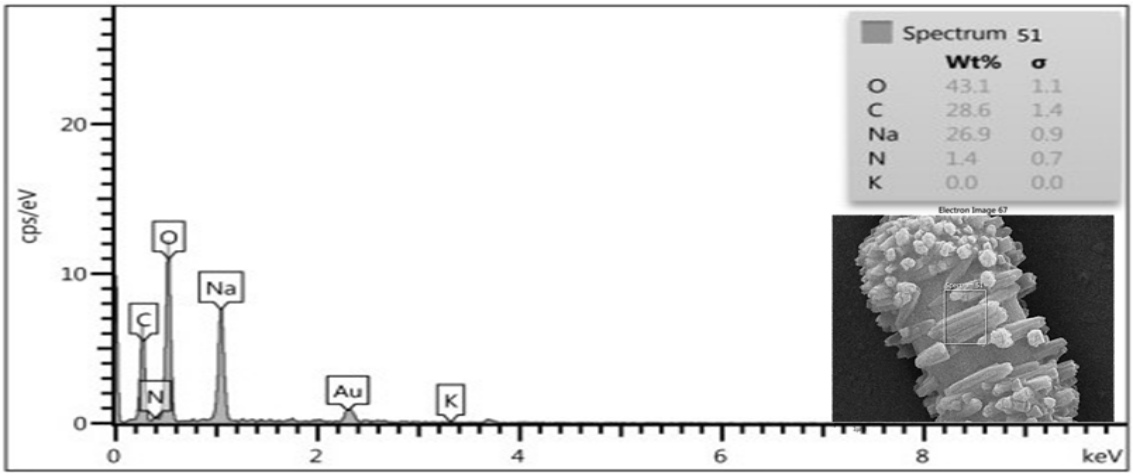


**Figure 6**.Spectrum of elemental analysis of CNPs loaded *T.harazanium* showed five main peaks by EDX, EDX analysis was performed via EDX Oxford instruments INCA 350 with Si detector 10mm2 area, resolution at Mn 133eV

### *3.3.5. Atomic Force Microscopy (AFM)*

The Atomic Force Microscopy (AFM) investigation for Chitosan nanoparticles (CNPs) laden with *T. harzianum* extract, as depicted in Figure 7, establishes the presence of homogenous sphere-like structures with a medium diameter of 33.62 nm, aligning with the dimensions derived from XRD outcomes. These observations affirm the existence of nano chitosan, attesting to its preferred structural configuration. Additionally, the analysis conclusively demonstrates that the surfaces exhibit nano chitosan characteristics, as portrayed in Figure 8, providing substantiation of the encapsulation with the fungal extract. This finding agrees with (Du *et al*., 2008); they showed that the biosynthesized chitosan nanoparticles were homogenous particles with an average size of 30–98 nm.

| Global statistics | | | | |
|---|---|---|---|---|
| Mean | ***** | 2469 | 33.62 | 1146 |
| Min | ***** | 123.0 | 7.748 | 1100 |
| Max | ***** | 119670 | 329.9 | 2365 |

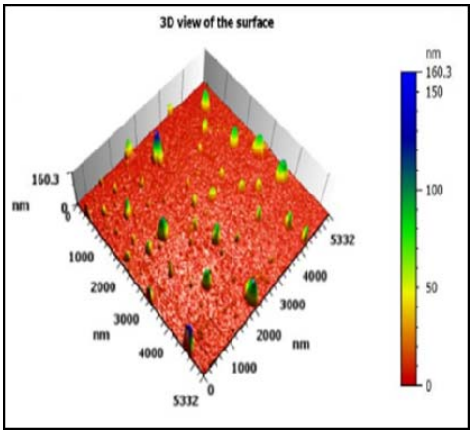


**Figure7**.Granularity distribution chart of CNPs loaden with T.harazanium extract based on particles size with a medium diameter of 33.62 nm surface morphology of the nanoparticles was visualized by Atomic Force Microscope Contact mode, under normal atmospheric conditions

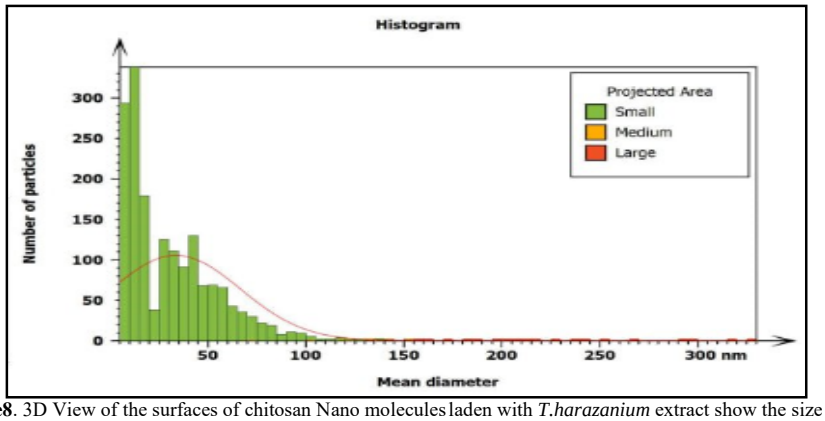


**Figure8**. 3D View of the surfaces of chitosan Nano molecules laden with *T.harazanium* extract show the size of particles

### 3.3.6. Analysis of Scanning Electron Microscopy

The exceptional dispersion and intricate morphology of Chitosan nanoparticles (CNPs), resulting in an increased exposed surface area, are discernible in the three-dimensional scanning electron microscopy (3D SEM) image. This observation further substantiates the suitability of CNPs for adsorption purposes. The analysis revealed a distinctive geometric structure for the CNPs laden with *T. harzianum* extract composite, illustrating the presence of uniformly shaped spherical structures with diameters ranging from 17.86 to 31.26 nm, indicative of Nano chitosan and affirming the success of encapsulation (refer to Figure 9). These porosity and aggregated CNPs have been identified as crucial characteristics for the manufacturing of innovative CNPs to enhance their efficacy as biologically synthesized nanomaterials in the applications of agriculture. The porous nature of these CNPs facilitates the effective adsorption of harmful chemicals and the suppression of pathogens. Notably, high-porosity nanoparticles exhibit greater specific external area and heightened reaction activity compared to lower-porosity bulk materials (Khan, 2019). The ratio of TPP to chitosan determines the size of the nanoparticles. To create nanoparticles, TPP, a positive charge ion, combines with the chitosan's negatively altered amino group. Previous studies indicate that altering the chitosan to stabilizer ratio can change the size and surface of chitosan nanoparticles (Deshaies *et al.,* 2022)

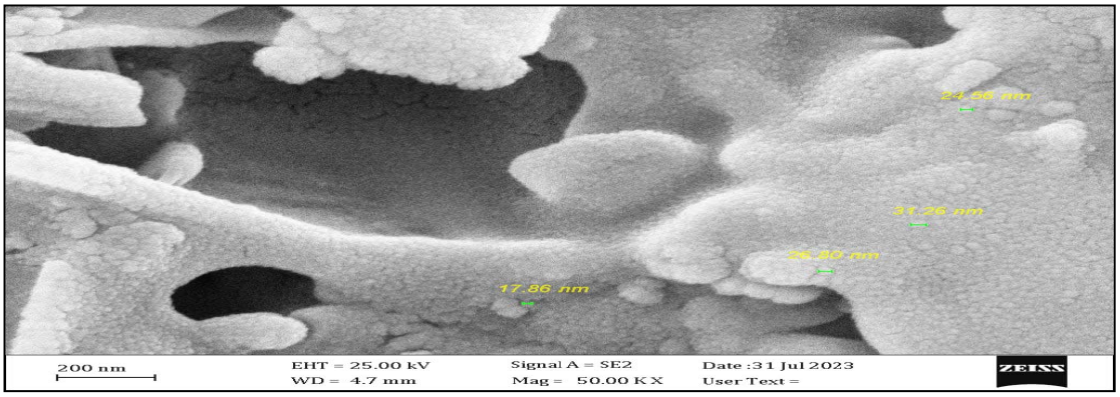


**Figure 9**. Image from Scanning Electron Microscopy showed the shape and size of chitosan nanomolecules laden *T. harazanium* extract , illustrating the presence of uniformly shaped spherical structures with diameters ranging from 17.86 to 31.26 nm

### 3.4. Antifungal Activity of CNPs Laden T. harzianum Extract

Utilizing Chitosan nanoparticles (CNPs) as a biodegradable polymer, the in vitro antifungal efficacy of CNPs laden with *T. harzianum* extract demonstrated significant inhibition of *F. oxysporum* f.sp. *lycopersci* growth in the PDA medium. The reaction occurring in the cationic amino groups of CNPs and fungal cellular constituents together suggests inherent antifungal properties (Deshaies *etal*., 2022). Each experiment has been conducted in a PDA medium with varying CNP concentrations ranging from 0.125 to 1 mg/ml, at room temperature for 168 hours. Figure 10 and Table 2 illustrate the impact of CNPs laden with *T. harzianum* extract on the mycelium radial growth for five isolates of *F. oxysporum* f.sp.*lycopersci.* The results indicate that elevating CNPs concentration correlates with increased inhibition percentages for all isolates (Huang, 2021). The highest inhibition rates of mycelium radial growth for all isolates were observed at 100% for a CNPs amount of 1 mg/ml, while the minimum inhibition rates for the five isolates were 32.75, 32.83, 32.85, 36.92, and 41.17% at a CNPs concentration of 0.125 mg/ml, consecutively. In comparison, the recommended dosage of Topsin fungicide (positive control) resulted in nearly 100% inhibition of fungal growth.

The concentration of chitosan directly correlates with the level of fungicidal effectiveness; previous research has shown that chitosan derivatives inhibit the growth of several plant-pathogenic fungi (Abdulateef *et al*., 2023). These results were similar to those found by Du *et al.* (2008) who reported that nano-chitosan was effective and gave promising antifungal activity at a lower concentration of 1000 ppm against *F. solani* and *F. oxysporum*, with a fungal growth inhibition rate of 41.48 and 30.37%, respectively. These results were also consistent with those found by Boruah and Dutta (2021), who mentioned that CNPs synthesized using *T. asperellum* were effective in inhibiting the growth of *F. oxysporum* and other soil-borne pathogenic fungi.

The ability of nano chitosan may be directly related to the activity of enzymes (catalase and peroxidase), which control the balance of reactive oxygen species (ROS) for plant resistance, and this led to a significant reduction in disease severity (Dheeb *et al.* 2015). Plant pathogenic fungi have varying levels of tolerance to chitosan nanoparticles (Al-Sarraj, 2024; Kaur *et al*., 2012; El-Mohamedy *et al.,* 2014).

It is crucial to note that variations in experimental conditions and fungal types may contribute to discrepancies between the findings of the present investigation *F. oxysporum* f.sp. *lycopersci* has been effectively inhibited by CNPs, suggesting potential strategies to impede sporogenesis, spore germination, and mycelia development. Three proposed mechanisms elucidate chitosan's inhibitory action. First, chitosan primarily targets the fungal cell membrane, increasing permeability and leading to the leakage of cellular contents, ultimately inducing cell death. The modification of membrane permeability and its interaction with the

fungal cell membrane may underlie chitosan's inhibitory effect.

In the second strategy, chitosan's chelating action binds trace elements, preventing their utilization for fungal development. Lastly, the positive charge of chitosan facilitates interaction with the negatively charged phospholipid elements of the fungal cell membrane, potentially disrupting proteins or DNA within fungi, and hindering the synthesis of necessary proteins and enzymes by preventing mRNA synthesis (AL Karagholy 2017).

**Table2**. The Impact of Chitosan Nanoparticles Laden with *T. harzianum* Extract on the Growth Inhibition Percentage of the Investigated Isolates.

| CNPs laden *T.harzianum* extract conc.(mg/ml ) | Mean ±SE of Inhibition Percentage of fungal growth (%) | | | | |
|---|---|---|---|---|---|
| | *F.oxysprum*3 | *F.oxysprum*5 | *F.oxysprum*9 | *F.oxysprum*17 | *F.oxysprum*20 |
| C: 0.125 | 41.17 ±2.07 d | 32.75 ±1.97 d | 32.85 ±2.19 d | 32.83 ±1.87 d | 36.92 ±1.69 d |
| C: 0.25 | 58.82 ±2.65 c | 58.62 ±2.61 c | 61.42 ±3.08 c | 58.2 ±2.05 c | 64.61 ±2.97 c |
| C: 0.5 | 75.0 ±3.96 b | 74.13 ±3.56 b | 74.28 ±4.05 b | 76.11 ±3.54 b | 78.46 ±3.55 b |
| C: 1 | 100 ±0.00 a | 100 ±0.00 a | 100 ±0.00 a | 100 ±0.00 a | 100 ±0.00 a |
| Control Topsin (+ve) | 100 ±0.00 a | 100 ±0.00 a | 100 ±0.00 a | 100 ±0.00 a | 100 ±0.00 a |
| Control(- ve) | 68 ±3.72 e | 58 ±2.96 e | 70 ±3.05 e | 67 ±3.56 e | 65 ±3.61 e |
| LSD value | 8.77 ** | 8.65 ** | 9.02 ** | 8.61 ** | 8.69 ** |

** (P≤0.01).

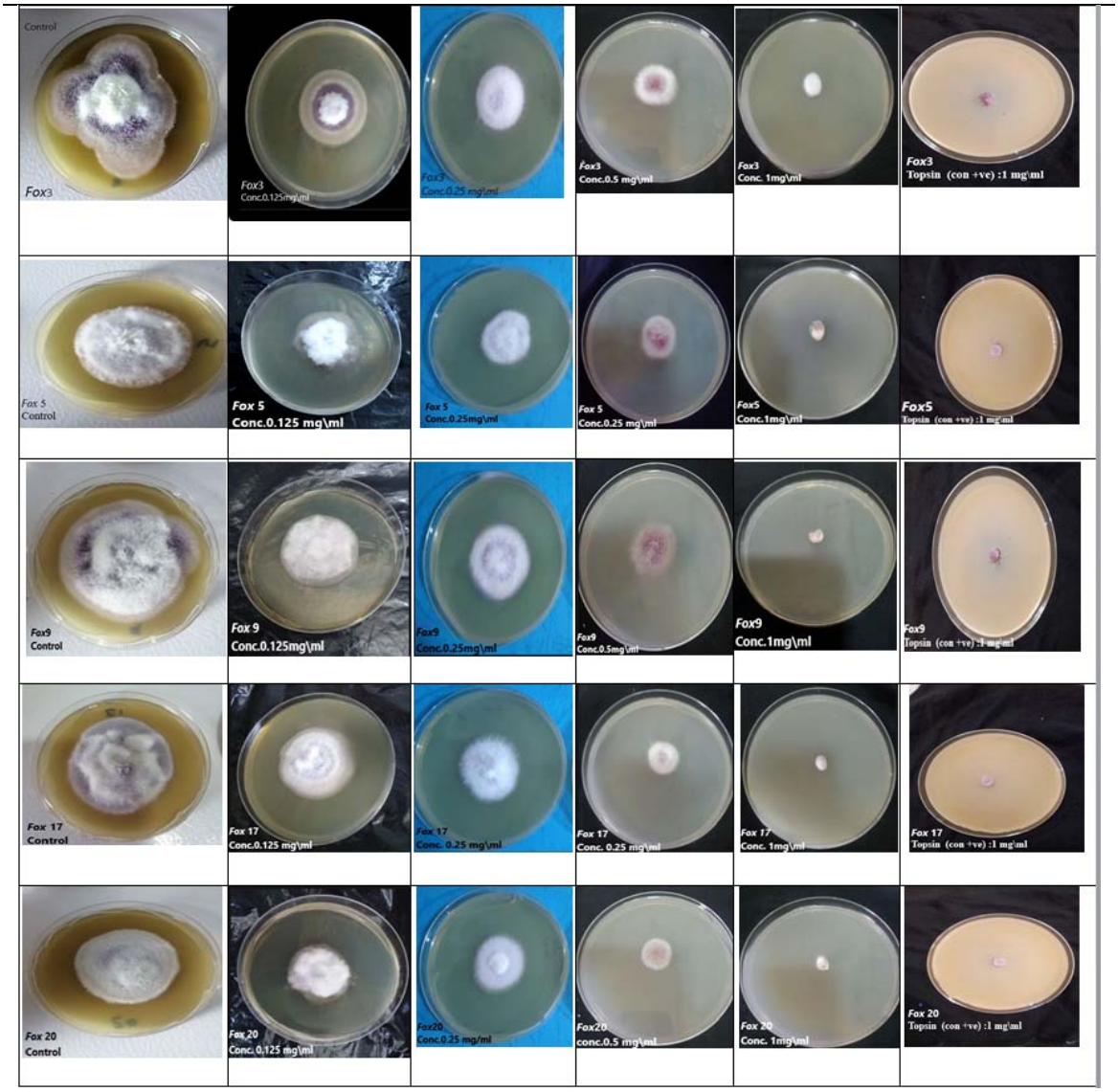


**Figure10**. Antifungal activity of Chitosan nanoparticles loaded with *T.harazanium* extract against *F.oxysporum* f.sp.*lycopersci*

## 4. Conclusions

The present investigation introduces a new eco-friendly method employing *T. harzianum* extract for the eco-friendly manufacturing of CNPs. The comprehensive characterization for the CNPs substantiates the efficacy and suitability of *T. harzianum* extract as a bio-transforming agent. The demonstrated antifungal efficacy of the synthesized CNPs towards *F. oxysporum* underscores their potential as alternatives to or mitigators of the widespread use of chemical fungicides. Moreover, their versatility extends to diverse applications in both technical and agricultural domains.

## References


Abdulbaqi N J , Dheeb, B I and Irshad R. 2018. Expression of biotransformation and antioxidant Genes in the Liver of Albino Mice after exposure to aflatoxin B1 and an Antioxidant Sourced from Turmeric (Curcuma longa). *Jordan J Biol Sci*., **11(2) :** 89 – 93.

Abdullah HI, Hammadi SY, Hussein AS, Dheeb BI .2019. Investigation of genetic diversity and relationships among the clinical candida species using random amplified polymorphic DNA (RAPD) analysis. *Research J of Biotech.*, **14(1):**6–13.

Abed FD, Saadedin S MK and Shareef HK. 2021. Molecular deduction of *Aspergillus flavus* isolated from wheat grains in Karbala city. *Iraqi J of Biotech.* ,**20(1):**46-53.

Abed SM, Farhan MG, Madhloom NK, DheebDI. 2022 .Magnetic Field Exposure to Clinical Isolates of Acinitobacter baumanii. *Biomed .Pharmacol. J*., **15(4):**5-17

Agarwal MK, ShrivastavN, PandeyS, Das R and Gaur P. 2018. Preparation of chitosan nanoparticles and their In-vitro characterization. *Int. J. Life Sci. Scienti. Res.* **4(2):**1713–1720.

AL Karagholy K A .2017. Chitosan and keratin hydrolysate treatment of archived newsprint. *Ibn AL-Haitham J. for Pure and Appl. Sci.* , **23(1):** 180–188.

Aldobaissi IAM and Almasoudi RKH. 2021. Study of fruits morphological features for 33 species belong to Cruciferae family in Iraq . *Iraqi J. Agric. Sci.* , **52(4):** 1039–1049.

Alqaysi S,Aldeen AS and Alwan AH. 2016 .Molecular identification of rhizosphere *Trichoderma* spp. and their antagonistic impact against some plant pathogenic fungi. *Baghdad Sci. J.,* **13 (1):** 53-65.

Awad FM, Al-Samarrai AHM, Dheeb BI. 2020 .Study of the inhibitory effects of rheum ribes extracts on a pathogenic fungi and cancer cell line. *Plant Archives*, **20(1):** 3161–3168.

Abdulateef S M, Ibraheem S, Hussein H S, Dheeb BI, Khashman BM, Ahmed DM, Abu-Elteen KH . 2024. MMP-1 and MMP-7 expression is influenced by ginsenosides in mice exposed to aflatoxin B1: in vivo study. *Jordan J. of Pharm. Sci*., **17 (1):** 135-1139.

Al-Sarraj BM, Massadeh MI, Dheeb BI. 2024. Bacteriological and Molecular Detection of Fluoroquinolone Resistance in *Escherichia coli* Isolated from Women Patients with urinary Tract Infections. *farmacia*., **27(4):**840-842.

Boruah S and Dutta P. 2021. Fungus mediated biogenic synthesis and characterizat- upon of chitosan nanoparticles and its combine effect with *Trichoderma asperellum* against *Fusarium oxysporum, Scleroium rolfsii* and *Rhizoctonia solani*. *Indian Phytopath.,* **74(1):**81–93

Demchenko V, Riabov S, Sinelnikov S, Radchenko O, Kobylinskyi S and Rybalchenko N. 2020.Novel approach to synthesis of silver nanoparticles in interpolyelectrolyte complexes based on pectin, chitosan, starch and their derivatives. *Carbohydr Polym*. **242**:116431.

Deshaies M, Lamari N, Ng CKY, Ward P and Doohan FM. 2022. The impact of chitosan on the early metabolomics response of wheat to infection by *Fusarium graminearum*. *BMC Plant Biol.* , **73(22):** 1–17.

Dheeb B I, Abdulla S N, Shanter ALQaysi, S A, Al-Sarraj B M and Farhan M S. 2023. Extraction of *Klebsiella pneumoniae* and *Candida albicans* biofilm and studying their cytotoxic effects on human lymphocytes. *Jordan J Biol Sci.*,., **16(4):** 717 – 726.

Dheeb B I, Al-Mudallal N H, Salman Z A and Ali M. 2015. The Inhibitory Effects of Human, Camel and Cow's Milk against Some Pathogenic Fungi in Iraq. *Jordan J Biol Sci.,* **8(2):** 89 – 93.

Dheeb BI, Hashim SS, Hussein HS, Hamada TA.2022. Study of TGF- β Immune Marker Expression in Mice Exposed to Candida Spp. *AIP Conf. Proc.,* Vol (**2394):1**.

Du W L, Xu Z R,Han XY, Xu Y L and Miao Z G .2008. Preparation, characterization and adsorption properties of chitosan nanoparticles for eosin Y as a model anionic dye. *J. of Haz.Mat.* , **153(2):** 152–156.

El Naggar N E, Saber WIA , Zweil A M and Bashir SI. 2022. An innovative green synthesis approach of chitosan nanoparticles and their inhibitory activity against phytopathogenic *Botrytis cinerea* on strawberry leaves. *Sci. Rep.,***12(1):**3515.

EL Sayed ME, Yomna S E and Mohamed MA M. 2023. Biocontrol of *Fusarium equiseti* using chitosan nanoparticles combined with *Trichoderma longibrachiatum* and *Penicillium polonicum. Fungal Biol and Biotech.*, **10(5)** : 1-8

El-Mohamedy RS, Abdel-Kareem F, Jaboun-Khiareddine H and Daami-Remadi M. 2014. Chitosan and *Trichoderma harzianum* as fungicide alternatives for controlling Fusarium crown and root rot of tomato. *Tunisian J. of Plant Pro..,* **9(1):** 31-43.

Esmael Majed R,Ali Hadwan H, Adel Abed H, Mansor Hamza M,Faris Hasen O and Hmood Ali E. 2021. Estimate different bioagent as A biofertilizer with two level from chemical fertilizer on wheat crop improvement. *Iraqi J. of Sci*., ***58*(4B):**2035–2040.

Farahani-Kofoet RD, Witzel K, Graefe J, Grosch R and Zrenner R. 2020. Species-specific impact of *Fusarium* infection on the root and shoot characteristics of asparagus. *Pathogens.*, **9(6) :** 1 - 20.

Fradi A J .2022.The Effective concentration of the crude extract of *Mentha picata* and *Eucalyptus* against the growth of *Fusarium oxysporum*. *Ibn Al-Haitham J.For Pure and Appl. Sci.* , **35( 4):** 1-8.

Hashim S S, Mahmood Z F, Abdulateef S F, Dheeb B I. 2023. Evaluation Cytotoxicity Effects of *Centaurea Cineraria* Extracts Against some of Cancer Cell Lines. *Biomed .Pharmacol. J.,* **16(1):**3-17 .

Huang X, You Z, Luo Y, Yang C, Ren J, Liu Y, Wei G, Dong P and Ren M. 2021.Antifungal activity of chitosan against *Phytophthora infestans*, the pathogen of potato late blight. *Inter.J. of Biol. Macro*.,**166(1)**: 1365-1376

Hussain AF, Sulaiman GM, Dheeb BI , Hashim AJ. 2018. Histopathological changes and expression of transforming growth factor beta (TGF-β3) in mice exposed to gliotoxin. *J. of K S U Sci*., **27(12):** 193–197.12.

Jasim SF, Abdulbaqi NJ, Al-Zubaidi LA and Jasim AD. 2022.Evaluation of atmospheric cold plasma technique activity on phenylpropanoids gene expression and essential oil contents and different traits of *Ocimum basilicum* L. *Baghdad Sci. J.,* **19(5):**966–975

Juber KS. 2012. Evaluating the virulence of some pathogenic isolates for three *Fusarium* species in Date- palm and their control. *Iraqi J. Agric. Sci.*, **43( 2):**7-17.

Kareem H J and Al-Araji A M. 2021. Evaluation of *Trichoderma Harzianum* Biological control Against *Fusarium oxysporum* F. Sp. *Melongenae*. *Iraqi J. of Sci.*, ., **58(4B):** 2051–2060.

Kaur P, Thakur R and Choudhary A. 2012. An in-vitro study of antifungal activity of silver/chitosan nanoformulations against important seed borne pathogens. *Int. J of Sci. & Techn. Res*., **1(6):** 83-86.

Khan, I., Saeed, K. & Khan, I. (2019).Nanoparticles: Properties, applications and toxicities. *Arabian J. of Chem* **., 12(7) :** 908-931

Mahdavi V, Saber M, Dastjerdi HR. And Mehrvar A. 2013.Susceptibility of the Hymenopteran Parasitoid, Habrobracon hebetor (Say) (Braconidae) to the Entomopathogenic Fungi Beauveria bassiana Vuillemin and Metarhizium anisopliae Sorokin. *Jordan J Biol Sci.,* **6 (1)**: 17-20

Medda S, Hajra A, Dey U, Bose P and Mondal N K. 2015. Biosynthesis of silver nanoparticles from Aloe vera leaf extract and antifungal activity against *Rhizopus* sp. and *Aspergillus* sp. *Appl. Nanosci.*, **5(7):** 875-880.

Morsy M, Mostafa K, Amyn H, El-EbissyA A H, Salah A M and Youssef M A. 2019. Synthesis and characterization of freeze dryer chitosan nano particles as multi-functional eco-friendly finish for fabricating easy care and antibacterial cotton textiles. *Egypt. J.of Chem.* **, 62(7):** 1277-1293.

Mustafa HNand Al –OgaidiI. 2023. Efficacy of zinc sulfide – chitosan nanoparticles against bacterial diabetic wound infction . *Iraqi J. Agric. Sci.*, **54(1):**1–17.

Oh J W, Chun S C and Chandrasekaran M. 2019.Preparation and in vitro characterization of chitosan nanoparticles and their broadspectrum antifungal action compared to antibacterial activities against phytopathogens of tomato. *Agronomy*., **9(1):** 21-31.

Rabea EI, Badawy M E I, Steurbaut Wand Stevens CV. 2009. In-vitro assessment of N-(benzyl) chitosan derivatives against some plant pathogenic bacteria and fungi. *Eur. Polym. J.*. , 45**(1):** 237–245.

Raza Z A and Anwar F. 2017. Fabrication of chitosan nanoparticles and multi-response optimization in their application on cotton fabric by using a Taguchi approach. *NanoStru.s and Nano-Obj.*, **10**: 80–90.

Salih, II, Seddiq SH, Hashim SS, Dheeb BI . 2022.Application of Omics and Proteomics in Fungi. *AIP Con.Proc.,* Vol. **(2394):1.**

SAS 2018. **Statistical Analysis System, User's Guide. Statistical**. Version 9.6th ed. SAS. Inst. Inc. Cary. N.C. USA,

Thamilarasan V, Sethuraman V, Gopinath K, Balalakshmi C, Govindarajan M, MothanaR A, Siddiqui N A, Khaled J M and Benelli G. 2018. Single step fabrication of chitosan nanocrystals using Penaeus semisulcatus: potential as new insecticides, antimicrobials and plant growth promoters. *J of Clus. Sci.* , **29(2):** 375-384.

Thomas S, Thomas R, Zachariah AK and Mishra RK.2017. Spectroscopic Methods for Nanomaterials Characterization.In: Dutta A (Eds.), **Fourier Transforms Infrared Spectroscopy**. Elsevier Publishers, pp. 73-93.

Zhao X H, Li N N, Xu J, Dong X Y, Li S and Zang S Q. 2023. Pseudorotaxane ligand-induced formation of copper (I) iodide cluster based assembly materials: from zero to three dimensional. *Chin. J of Chem*., **41(16):** 1943-1949.